Energy & Buildings 248 (2021) 111210

Contents lists available at ScienceDirect

Energy & Buildings

journal homepage: www.elsevier.com/locate/enb

Fast simulation and high-fidelity reduced-order model of the multi-zone radiant floor system for efficient application to model predictive control

Qiong Chen, Nan Li *

National Centre for International Research of Low-carbon and Green Buildings, Ministry of Science & Technology, Chongqing University, Chongqing 400045, China

ARTICLE INFO

Article history:
Received 18 April 2021
Revised 11 June 2021
Accepted 20 June 2021
Available online 24 June 2021

Keywords:
Model order reduction
Balanced truncation method
Radiant floor system
Model predictive control
Building simulation

ABSTRACT

Model predictive control, as the most popular intelligent advanced control technology in recent years, is increasingly applied to building air conditioning systems to achieve adaptive and energy-efficient operation of the system, however, model predictive control imposes higher requirements on the computational efforts of the model. In this research, a complex coupled heat transfer model of the increasingly popular radiant floor system is analyzed and a full-order model of the radiant floor is developed. Then, after controllability and observability analysis, a fast high-fidelity reduced-order model that can accurately characterize the dynamic thermal performance of the original model is proposed applying the balanced truncation method. The accuracy of the reduced-order model was verified by comparing the radiant floor surface temperature, return water temperature, zone air temperature, and unheated average internal surface temperature with experimental test results, the TRNSYS model, and the full-order model. The computation time of the reduced-order model for open-loop simulation was reduced by 86% to 98% compared to the TRNSYS model. More importantly, the reduced-order model can effectively reduce the complexity of the model predictive control, resulting in a 38% to 78% saving in computation time compared to the full-order model, significantly improving computational efficiency and enhancing the robustness of the model predictive control.

1. Introduction

In recent years, as radiant floor heating systems are more and more widely used in hot summer and cold winter regions of China, the application of model predictive control for such large time lag systems can significantly reduce the problems of increased system energy consumption and prolonged system thermal response time caused by the large thermal inertia of the system[1]. Secondly, model predictive control puts higher requirements on the computational power of the prediction model, and too much model computation will lead to the degradation of control system adaptiveness and robustness[2]. By simplifying the prediction model and reducing the computational volume of the prediction model in the rolling optimization process, it is an effective method for the energy-saving operation of radiant floor heating systems after applying model predictive control. Jiang Yi[3] has pointed out in his research that at least 30 states are generally needed to ensure the simulation accuracy of the state-space model single region of the thermal model. The more states of the model require more CPU time to complete the computation.

The excessive model order hinders the application of model predictive control[4], and there have been many pieces of research to apply the mature order reduction method in control systems to building models, such as building envelope[5,6], single-zone[7,8] or multi-zone building models[9,10], etc. Applying this method to building models greatly simplifies the model structure and reduces the model computation while reducing the model dimensionality, which has unprecedented significance in the field of model predictive control research[11]. Nowadays, model reduction methods have started to be applied to more complex mathematical and physical models, such as fluid models, electromagnetic field models, etc.[12]. In the numerical solution of various partial differential equations, model reduction methods are widely used because of their fast computational speed and high computational efficiency[13–15].

The applicability of the harmonic response method, Krylov subspace method, and balanced truncation method in the building envelope model was compared and analyzed by Qiong Xiangkong et al.[16] through numerical simulations. The simulation results show that the decrement coefficients as well as the peak and valley

* Corresponding author.
E-mail address: nanlicqu@163.com (N. Li).

https://doi.org/10.1016/j.enbuild.2021.111210
0378-7788/

Nomenclature

m^{sp}	Mass flow per unit of area
c_w	Specific heat capacity of water
R_w	Convective thermal resistance on the inner surface of the heat pipe
R_r	The conductive thermal resistance of the heat pipe
R_x	The conductive thermal resistance of the radiant floor core layer
U_1	Heat transfer coefficient of the upper configuration of the core layer
U_2	Heat transfer coefficient of the lower configuration of the core layer
Nu	Nusselt number
λ_w	Thermal conductivity of water
λ_r	Thermal conductivity of the heat pipe
λ_b	Thermal conductivity of the core layer
L	Length of heat pipes
d_o	External diameter of the heat pipe
d_i	The internal diameter of the heat pipe
d_x	Pipe spacing of heat pipes
σ	Stefan-Boltzmann
ε	Surface emission rate
$F_{i,j}$	Radiant angle factor
C_f	Heat capacity matrix of the radiant floor
C_w	Heat capacity matrix of the building envelope
C_{air}	Heat capacity matrix of the zone air
H_f H_{fw} H_{fz}	Matrix of heat transfer coefficients of the radiant floor
H_w H_{wf} H_{wz}	Matrix of heat transfer coefficients of the building envelope
H_z H_{zf} H_{zw}	Matrix of heat transfer coefficients of the zone air
T_f	Vector of temperature nodes of the radiant floor
T_w	Vector of temperature nodes of the building envelope
T_z	Vector of temperature nodes of the zone air
q_f	Heat flow matrix for the radiant floor
q_w	Heat flow matrix for the building envelope
q_z	Heat flow matrix for the zone air
q_{rad}	Radiant heat exchange
W_c	Controllability Gram matrix
W_o	Observable Gram matrix
Γ	Hankel matrix

values of the reduced-order model match the results of the harmonic response method when the roof model is simplified with these two reduced-order algorithms. The maximum absolute errors of temperature and heat flux calculated among these three models are 0.2 °C and 1.5 W/m^2, respectively. The Krylov subspace method is computationally fast, while the balanced truncation method has a better stability. Qiongxiang Kong et al.[17] conducted a comparative analysis of the application of the Krylov subspace method and balanced truncation method in building envelope model order reduction. The numerical simulation results of the building heat transfer models through the single roof, multilayer wall, and L-shaped thermal bridge showed that the relative errors of the reduced-order model by the two methods were less than 1% compared to the conventional harmonic response method but consumed much less computational effort. It was further found that the reduced-order model built by applying the Krylov subspace algorithm was computationally faster than that built by the balanced truncation method.

Hou Tianfeng et al.[18] investigated the performance of two reduced-order modeling methods, orthogonal decomposition (POD) and proper generalized decomposition (PGD), with the standard finite element method (FEM) in terms of computational accuracy and computational effort. The simulation results show that the POD model has higher computational accuracy than the PGD model and the FEM model. Besides, the POD method has higher applicability, better robustness, and flexibility for different building model downscaling simulation problems. Alexandra and Tallet[19] proposed a model reduction technique based on the proper orthogonal decomposition (POD) algorithm to model the infiltration air heat load of a building by introducing an infiltration heat recovery (IHR) factor in the energy balance equation. This newly proposed reduced-order model offers significant computational time savings compared to computational fluid dynamics (CFD) models and has been successfully applied to low-energy buildings.

Establishing a low-order building thermodynamic model is important for model predictive control (MPC), which is computationally demanding, and can greatly improve the computational efficiency of MPC[20]. Sidhash-Goyal[21] proposed a new method to reduce the order of a multi-zone dynamic temperature and humidity building model. Most of the order reduction techniques have many excellent applications in linear system models, but there are some limitations when applied to nonlinear systems. A novel method based on the balanced truncation method is proposed to solve the order reduction problem of nonlinear building models. The simulation results show that the order of the model is greatly reduced, the computational workload is reduced by more than 6 times, and the performance of the simplified model for predicting air temperature and humidity is almost the same as that of the full-order model.

Eui-JongKim[22] proposed a method to solve the simplified model directly using the balanced truncation method, which reduces the large number of iterations required to calculate the annual load of the Dymola model, thus improving the computational speed and also ensuring the accuracy of the model. The two-order simplified model of the direct solver was used to simulate ten buildings to verify that the reduced-order model could accurately predict the annual heat load of the buildings with a relative error of about 0.43% with the reference model. Ben Lyons et al.[23] combined the balanced reduction method based on Hankel singular value decomposition with the building energy modeling tools for the application of model predictive control (MPC) for a large number of building models. The MPC control schedule was developed for a space heating system of 95m^2-area zone as an example.

Previous studies mainly focused on model reduction methods for various building dynamic models, mainly including Krylov subspace method, orthogonal decomposition method, multi-point fitting model reduction method, balanced truncation method, and integral allometric transformation method, pade approximation method, time moment method, continuous fractional method, Ruth approximation method, etc[19,24,25]. Among them, the Krylov subspace method [19,24,25], the orthogonal decomposition method[26,27], the balanced truncation method [17,29,30], etc. Among them, the Krylov subspace method [16,17,26], the orthogonal decomposition method [27,28], and the balanced truncation method [17,28,29] are mainly applied in the field of thermal and humid building models.

Commonly used software for building simulation includes Computer Fluid Dynamics (CFD), EnergyPlus, and TRNSYS, which

characterizing the heat and mass transfer of building envelopes based on many differential equations, resulting in many iterations and low computational efficiency. Nowadays, more and more researchers apply the model reduction technique to the field of building engineering to reduce the dimensionality of the building model by eliminating the states meaningless to the system outputs. The reduced-order model can maintain the dynamic characteristics of the physical model of the building and greatly reduce the computational efforts of the numerical simulation, improve the computational efficiency and save the data storage space of the computer.

Radiant floor heating systems are large time-delay systems with severe thermal inertia of the building envelope, which seriously limits the real-time response performance of the control system [30]. The model predictive control system can predict the dynamic performance of the system in the future time domain and effectively alleviate the problems of high energy consumption and slow thermal response of the system caused by large thermal inertia [21–23,31]. However, the model predictive control requires a tough computational effort of the model, and the excessive amount of model computational will jeopardize the adaptiveness and robustness of the system[32]. Therefore, it is necessary to reduce the order of the radiant floor model to improve the computational efficiency of the model predictive control system while ensuring the accuracy of the model prediction[33]. Currently, model predictive control has been increasingly used to improve the energy-saving operation of building air conditioning systems, but there is little research on model order reduction and model predictive control of radiant floor systems, which has great research and promotion value today when radiant floor systems are becoming more and more popular. which is highly valuable to explore when radiant floor systems are almost preferred by the vast majority of people for superior comfort.

In this research, the state-space model of the radiant floor system is established by deeply analyzing the three-dimensional heat transfer process of the radiant floor system. The state-space model has better scalability than the data-driven model with experimental data for the following reasons. For all the alternative models derived from the data-driven models, to decide which one is the best choice for the implementation of the model predictive control is of great challenge. Besides, the pre-simulation of the data selection and the training algorithm is also a time-consuming process. The physics-based model is more suitable for MPC because the reliable and enormous operation or training data is hard to obtain for the data-driven model construction in practice. And then the model is reduced in order based on the balanced truncation method. Based on the controllable and observable analysis results of the model, as well as the frequency domain response performance and Hankel singular value of the reduced-order model, an accurate and low-order model of the radiant floor system is obtained. The accuracy of the reduced-order model of the radiant floor is confirmed by comparison with field experimental tests, the commonly used energy simulation software TRNSYS, and the full-order model of the radiant floor system. The computational efficiency of the transfer function model (TRNSYS), the full-order model, and the reduced-order model under open-loop simulation conditions are compared and analyzed, and the computational effort of the full-order model and the reduced-order model for the model predictive control system are compared and analyzed, confirming that the reduced-order model can greatly reduce the computational effort of the model predictive control, improving the computational efficiency and the robustness of the model predictive control system.

1.1. State-space model for the radiant floor system

The state-space model of the radiant floor system established in this research mainly consists of a three-dimensional radiant floor model, building envelope model, and indoor air model. In this study, a physics-based modeling approach is applied, which has been increasingly used for building dynamic modeling since its innovative introduction[34]. Building models based on machine learning and parameter identification often rely entirely on historical operational data. To improve the accuracy of the models, these inverse modeling approaches spend a lot of time upfront on complex pre-processing of operational data to generate the datasets required for model training[35], and access to high-quality building operational data is particularly limited. Besides, determining which is the best model among the numerous candidate training models is highly contingent, resulting in lower generality and a significant reduction in model accuracy for the system under different operating conditions[36].

The three-dimensional heat transfer model of the radiant floor is shown in Fig. 1. The most complex three-dimensional radiant floor model is mainly composed of the heat transfer process in the direction of water flow in the pipe, convective heat transfer process on the pipe inner surface, heat conductive process through the pipe wall, heat transfer in the core temperature layer of the floor, and other structural layers of the floor such as backfill, leveling layer and surface decoration layer, etc. The thermal resistance in the direction of water flow in the pipe is derived by the heat balance principle, as shown in Eq. (1). The thermal resistance of the pipe's inner surface is related to the state of the fluid, and the thermal resistance of the inner surface in the laminar and turbulent flow states are shown in Eq.(2) and Eq. (3), respectively. The thermal conductivity process of the tube wall can be considered as the thermal conductivity along the cylinder wall, which is calculated as shown in Eq. (4). The results of the finite element analysis about the radiant floor show that there is a core temperature layer near 1/3*dx (dx is the tube spacing) from the buried tube of the floor, and the temperature is almost constant as Tc, and the thermal resistance of this heat transfer process is expressed by the core temperature layer thermal resistance Rx, which is calculated as in Eq. (5). The study shows that the temperature distribution of the structural layers beyond the core temperature layer is uniform, and each layer of the structure can be represented by a temperature node. Based on the thermoelectric analogy theory proposed by Hartnett, J.[37,38] and the heat balance equation of each temperature node, the three-dimensional state-space model of the radiant floor can be obtained, as shown in Eq. (6).Where C_f is the heat capacity matrix of the radiant floor, $\vec{T}_f$ is the temperature matrix of the radiant floor layers, $\vec{T}_w$ is the temperature matrix of the building envelopes, $\vec{T}_z$ is the temperature matrix of the zone air. H_f is the conductive heat transfer coefficient matrix of the radiant floor, H_{fw} is the radiant heat transfer coefficient matrix of the radiant floor, H_{fz} is the convective heat transfer coefficient matrix of the radiant floor, $\vec{q}_f$ is the heat flow matrix of the radiant floor, including the solar radiation on the surface of the radiant floor and the heat supply from the water flow in the buried pipes, etc.

$$R_z = \frac{1}{\dot{m}_{sp}\cdot c_w\cdot\left\{1-\exp\left[-\left(\dot{m}_{sp}\cdot c_w\cdot\left(R_w+R_r+R_x+\frac{1}{U_1+U_2}\right)\right)^{-1}\right]\right\}} - \left(R_w+R_r+R_x+\frac{1}{U_1+U_2}\right) \quad (1)$$

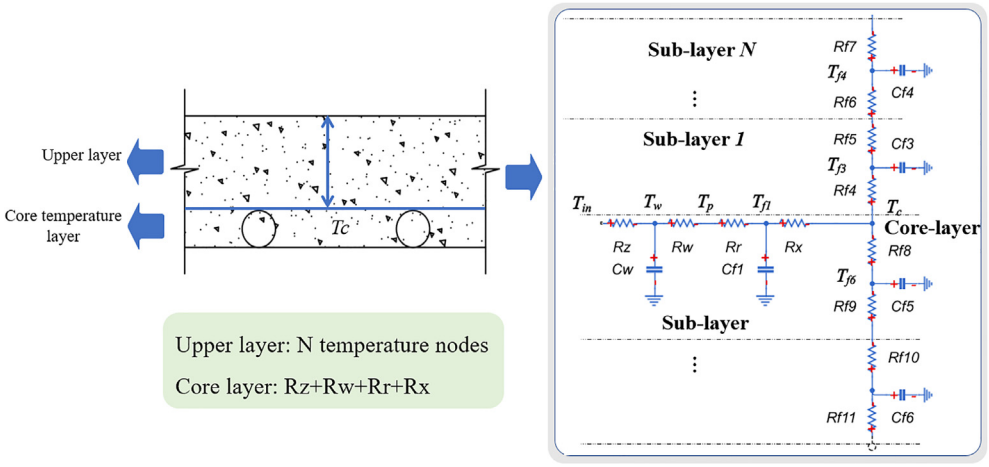

Fig. 1. The three-dimensional heat transfer model of the radiant floor.

$$R_w = 1/Nu * \lambda_w * \pi * L^2 * dx \tag{2}$$

$$R_w = \frac{d_x^{0.13}}{8.0 \cdot \pi} \cdot \left(\frac{d_i}{\dot{m}_{sp} \cdot l}\right)^{0.87} \tag{3}$$

$$R_r = \frac{d_x \cdot In\left(\frac{d_o}{d_i}\right)}{2 \cdot \lambda_r \cdot \pi} \tag{4}$$

$$R_x \approx \frac{d_x \cdot \frac{1}{3} \cdot \left(\frac{d_x}{\pi \cdot \delta}\right)}{2 \cdot \pi \cdot \lambda_b} \tag{5}$$

$$C_f \dot{\overrightarrow{T}}_f = H_f \overrightarrow{T}_f + H_{fw} \overrightarrow{T}_w + H_{fz} \overrightarrow{T}_z + \overrightarrow{q}_f \tag{6}$$

The conductive heat transfer model of the wall is shown in Fig. 2 (a). Each layer of the multi-layer enclosure is represented by a temperature node, and adjacent temperature nodes are connected by thermal resistance, and the heat capacity is used to represent the heat storage of the enclosure. The state-space model of the wall can be obtained, as shown in Eq. (7) by associating the heat balance equation of each temperature node, as shown in Eq. (8).

Where C_w is the heat capacity matrix of the building envelopes, H_w is the conductive heat transfer coefficient matrix of the building envelopes, H_{wf} is the radiant heat transfer coefficient matrix of the building envelopes, H_{wz} is the convective heat transfer coefficient matrix of the building envelopes, $\overrightarrow{q}_w$ is the heat flow matrix of the building envelopes.

For the outermost temperature node of the wall, there is convective heat exchange and solar radiation heat exchange with the outdoor environment. For the innermost temperature node of the wall, there exists convective heat exchange with indoor air temperature, convective heat dissipation and radiant heat exchange with indoor heat sources, and radiant heat exchange with other envelope surfaces, as shown in Fig. 3.

$$C_w \dot{\overrightarrow{T}}_w = H_{wf} \overrightarrow{T}_f + H_w \overrightarrow{T}_w + H_{wz} \overrightarrow{T}_z + \overrightarrow{q}_w \tag{7}$$

$$\begin{aligned} C_j \frac{dT_j}{d\tau} &= \frac{T_{(j-1)} - T_j}{R_{(j-1)2} + R_{j1}} + \frac{T_{(j+1)} - T_j}{R_{j2} + R_{(j+1)1}} \\ &= \frac{1}{R_{(j-1)2} + R_{j1}} T_{(j-1)} - \left(\frac{1}{R_{(j-1)2} + R_{j1}} + \frac{1}{R_{j2} + R_{(j+1)1}}\right) T_j \\ &\quad + \frac{1}{R_{j2} + R_{(j+1)1}} T_{(j+1)} \end{aligned} \tag{8}$$

The convective heat transfer model between the indoor air and the inner surface of the envelope is shown in Fig. 2(b). The heat balance equation of the indoor air temperature node is shown in Eq. (9), the state-space model of the indoor air temperature node can be obtained as shown in Eq. (10). Where C_{air} is the heat capacity matrix of the zone air, H_{zf} is the convective heat transfer coefficient matrix between the radiant floor and the zone air, H_{zw} is the convective heat transfer coefficient matrix between the building envelopes and the zone air, H_z is also the convective heat transfer coefficient matrix, $\overrightarrow{q}_z$ is the convective heat flow matrix, such as ventilation load and the infiltration load, etc.

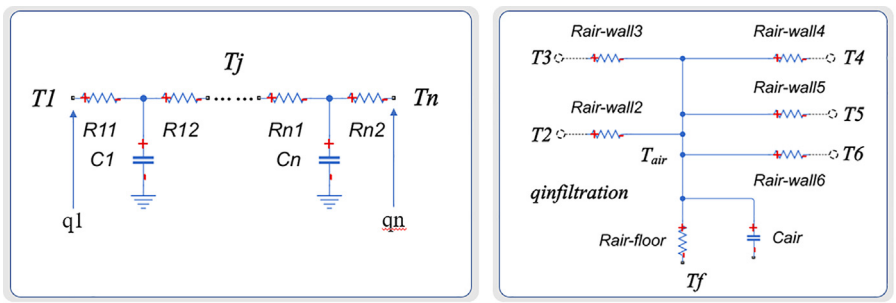

(a) conductive heat transfer model (b) convective heat transfer model of the indoor air

Fig. 2. Heat transfer model of the conductive, convective and convective heat transfer model.

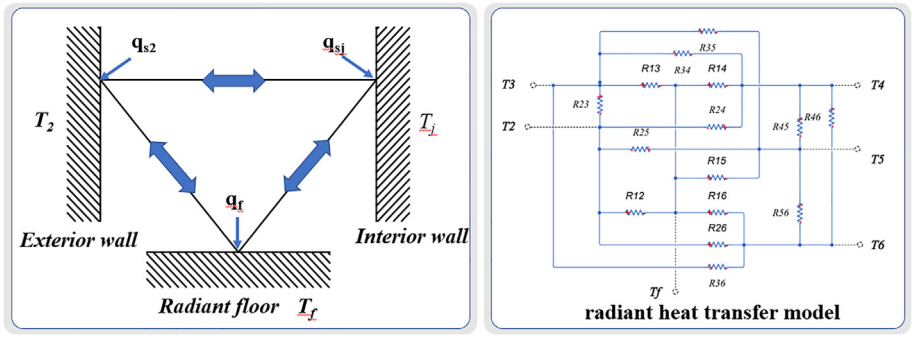

Fig. 3. Radiant heat transfer model of the internal surfaces.

$$\begin{aligned} C_{air}\frac{dT_z}{d\tau} &= Q_{surf,i} + Q_{inf} \\ &= \frac{T_{s1}-T_z}{R_{air-floor}} + \frac{T_{s2}-T_z}{R_{air-wall2}} + \frac{T_{s3}-T_z}{R_{air-wall3}} + \frac{T_{s4}-T_z}{R_{air-wall4}} + \frac{T_{s5}-T_z}{R_{air-wall5}} \\ &\quad + \frac{T_{s6}-T_z}{R_{air-wall6}} + Q_{inf} \\ &= \frac{T_f-T_z}{R_{air-floor}} + \sum_{i=1}^{5}\frac{T_{si}-T_z}{R_{air-walli}} + Q_{inf} \end{aligned} \tag{9}$$

$$C_{air}\dot{\vec{T}}_z = H_{zf}\vec{T}_f + \underset{zw}{H}\vec{T}_w + H_z\vec{T}_z + \vec{q}_z \tag{10}$$

By combining the state space heat transfer model of the radiant floor, building envelope, and indoor air, the state-space model of the radiant floor zone is obtained, as seen in Eq. (11).

$$\begin{aligned} \begin{bmatrix} \dot{\vec{T}}_f \\ \dot{\vec{T}}_w \\ \dot{\vec{T}}_z \end{bmatrix} &= \begin{bmatrix} C_f & 0 & 0 \\ 0 & C_w & 0 \\ 0 & 0 & C_{air} \end{bmatrix}^{-1} \begin{bmatrix} H_f & H_{fw} & H_{fz} \\ H_{wf} & H_w & H_{wz} \\ H_{zf} & H_{zw} & H_z \end{bmatrix} \begin{bmatrix} \vec{T}_f \\ \vec{T}_w \\ \vec{T}_z \end{bmatrix} \\ &\quad + \begin{bmatrix} C_f & 0 & 0 \\ 0 & C_w & 0 \\ 0 & 0 & C_{air} \end{bmatrix}^{-1} \begin{bmatrix} \vec{q}_f \\ \vec{q}_w \\ \vec{q}_z \end{bmatrix} \\ &= \begin{bmatrix} C_f & 0 & 0 \\ 0 & C_w & 0 \\ 0 & 0 & C_{air} \end{bmatrix}^{-1} \begin{bmatrix} H_f & H_{fw} & H_{fz} \\ H_{wf} & H_w & H_{wz} \\ H_{zf} & H_{zw} & H_z \end{bmatrix} \begin{bmatrix} \vec{T}_f \\ \vec{T}_w \\ \vec{T}_z \end{bmatrix} \\ &\quad + \begin{bmatrix} C_f & 0 & 0 \\ 0 & C_w & 0 \\ 0 & 0 & C_{air} \end{bmatrix}^{-1} F\,u \end{aligned} \tag{11}$$

The experimental platform of the radiant floor heating system is shown in Fig. 4. Based on the principle of establishing the state-space model of the radiant floor zone introduced above, the state-space model of this experimental platform is set up in Simulink, as shown in Fig. 5. The radiant heat exchange between the inner envelope surfaces is calculated using the radiosity method as shown in Eq. (12) [32], and the radiant heat exchange process is linearized according to Eq. (13). The state-space model of the radiant floor zones with four rooms includes 148 states, 14 model inputs, and 28 model outputs finally, as shown in Fig. 5(a). The inputs include the water supply temperature, ambient temperature, and other boundary-layer temperatures of the radiant floor, etc. The outputs include the surface temperature of the radiant floor and the unheated envelopes, and the zone air temperature, etc.

$$q_{rad} = A^{-1}\left[B'T_i - h_o\right] \tag{12}$$

$$q_{ij} = \sigma\epsilon F_{ij}\left(T_i^4 - T_j^4\right) = 4\sigma\epsilon F_{ij}\bar{T}_{ij}^3\left(T_i - T_j\right) \tag{13}$$

For the accuracy comparison of the state space model established in this study with commonly used building energy simulation software, a TRNSYS model of the same radiant floor system was also established as a reference, as shown in Fig. 5(b).

1.2. Model order reduction

Model order reduction methods were first proposed in control theory for large-scale integrated circuit (LSI) systems to provide the necessary system-level synthesis and verification, and the basic principle is to reduce the complexity of the model by reducing its dimensionality while maintaining its dynamic characteristics[39]. The lower-order building model obtained by downscaling the state-space model of the radiant floor zone established in the

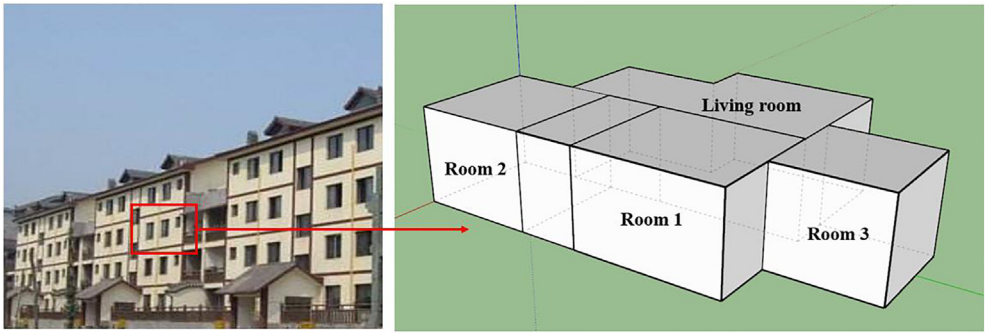

Fig. 4. Experimental building with four thermal zones for radiant floor heating systems.

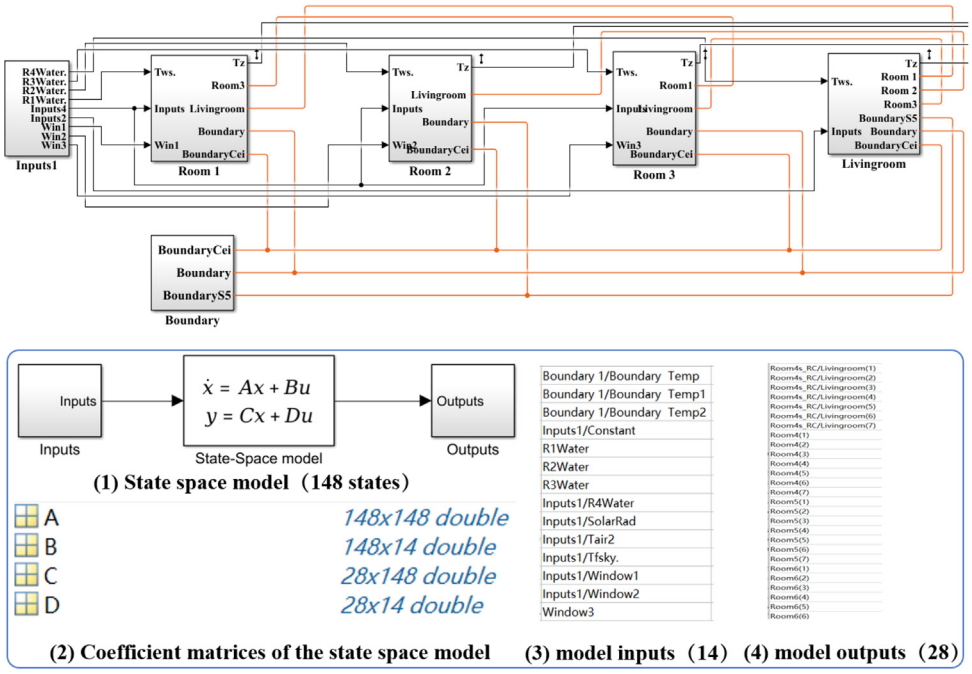

(a)

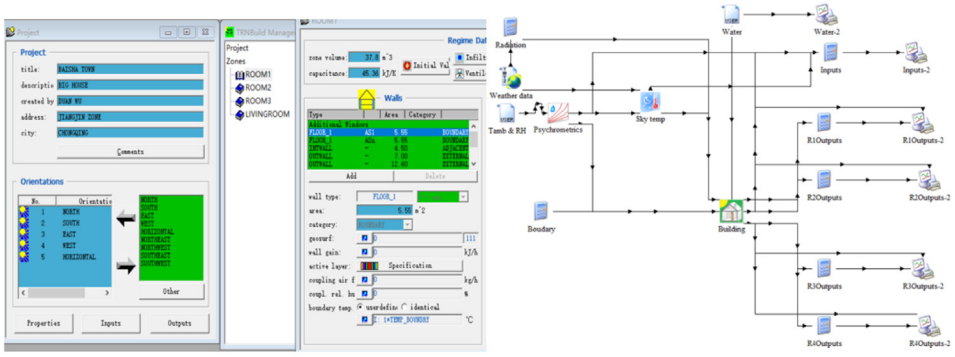

(b)

Fig. 5. (a) The state-space model in Simulink and (b) TRNSYS model of the radiant floor zones with four rooms.

above research is essential for improving the computational efficiency, shortening the computational time, and improving the dynamic response performance of the model predictive control. Based on previous studies, the balanced truncation method has been widely used in the existing building models order reduction research, and although the Krylov subspace method has a faster computational speed, it is better and more stable for systems of different nature applied with the balanced truncation method [40], which is the reason for choosing this method in this study [16,41].

A basic schematic diagram of the balanced truncation method and performance comparison of the reduced-order model with the response factor model is shown in Fig. 6. The controllability and observability analysis of the state-space model of the radiant floor zone is first performed before the downscaling of the state-space model. The state-space method applies to a wide range of control systems, such as adaptive control, optimal control, and model predictive control, etc[42]. The concepts of state space method, controllability, and observability for linear control systems were introduced by Kalman and laid the foundation of modern control theory[43].

For $\dot{\breve{x}}(t) = \breve{A}\,\breve{x}(t) + \breve{B}\,u(t)$, a system is controllable if, for any given input $\breve{x}(t_0)$ vector $u(t)$, it can be made to transfer from some initial state $\breve{x}(t_0)$ to any terminal state $\breve{x}(t_1)$ in a finite time interval $[t_0, t_1]$. According to the definition of controllability and the Cayley-Hamilton theorem[44], it is desired to transfer $\breve{x}(0)$ to $\breve{x}(t_1) = 0$ in $[0, t_1]$, i.e.

$$\breve{x}(t_1) = e^{At_1}\,\breve{x}(0) + \int_0^{t_1} e^{A(t_1-\tau)} B u(\tau) d\tau = 0 \tag{14}$$

$$-\breve{x}(0) = \int_0^{t_1} e^{-A\tau} B u(\tau) d\tau \tag{15}$$

$$e^{A\tau} = I + At + \frac{1}{2!}A^2t^2 + \cdots = \sum_{k=0}^{\infty} \frac{1}{k!}A^k t^k$$
$$= \alpha_0(t)I + \alpha_1(t)At + \cdots + \alpha_{n-1}(t)A^{n-1} = \sum_{k=0}^{n-1} \alpha_k(t)A^k \tag{16}$$

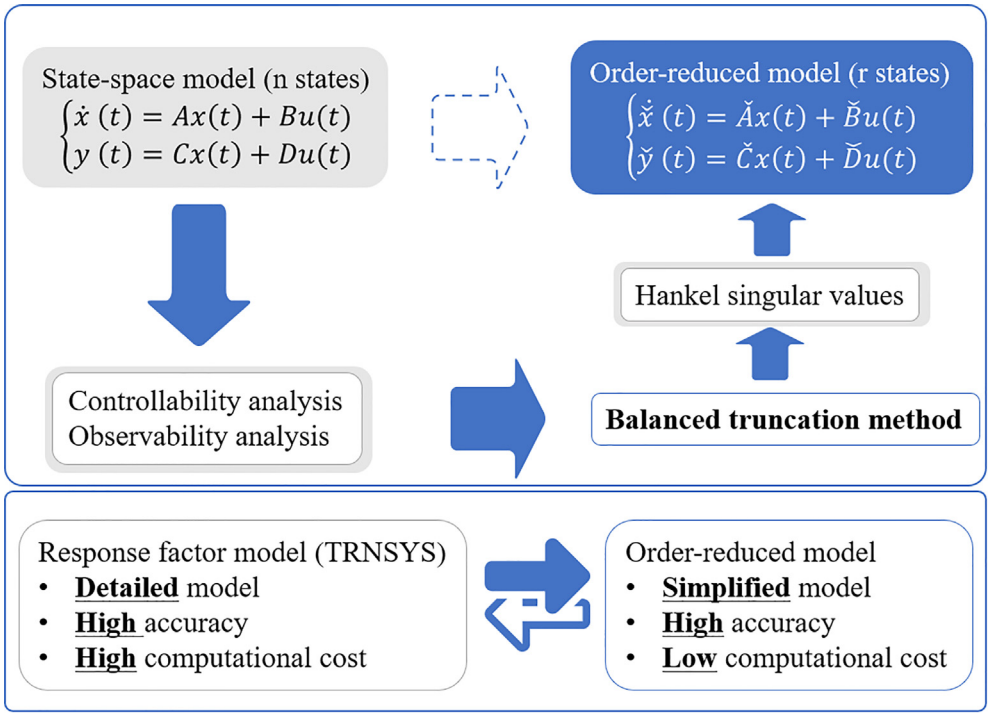

Fig. 6. Basic schematic diagram of the balanced truncation method, and performance comparison of the reduced-order model with the response factor model.

$$-\breve{x}(0) = \sum_{k=0}^{n-1} A^k B \int_0^{t_1} \alpha_k(t)u(\tau)d\tau = \begin{bmatrix} B & AB & \dots A^{n-1}B \end{bmatrix} \begin{bmatrix} \beta_0 \\ \beta_1 \\ \vdots \\ \beta_{n-1} \end{bmatrix} \tag{17}$$

$$\beta_i = \int_0^{t_1} \alpha_i(\tau)u(\tau)d\tau, i = 0, 1, \cdots, n-1 \tag{18}$$

Therefore, the sufficient condition for a linear time-invariant system to be fully controllable is $\mathrm{rankQ_c} = \mathrm{rank[BAB\cdots A^{n-1}B]} = \mathrm{n}$. Whether the system is controllable is uniquely determined by the two coefficient matrices A and B of the state-space model, reflecting the inherent properties of the system, independent of the system inputs, disturbances, and with the initial state. For a multi-input system, the simplified criterion is $\mathrm{rank[BAB\cdots A^{n-r}B]} = \mathrm{n}$, where r is the rank of the B matrix.

A system is observable if, for any given input $u(t)$, the initial state $\breve{x}(t_0)$ of the system can be uniquely determined from the measurements of the output vector y(t) for a finite time interval $[t_0, t_1]$. According to the definition of observability and the Cayley-Hamilton theorem[44], it is obtained as follows.

$$y(t) = Ce^{\mathrm{A(t-t_0)}}\breve{x}(0) + \mathrm{C}\int_{t_0}^{t_1} e^{\mathrm{A(t-\tau)}}Bu(\tau) \tag{19}$$

$$y(t) - \mathrm{C}\int_{t_0}^{t_1} e^{\mathrm{A(t-\tau)}}Bu(\tau) = Ce^{\mathrm{A(t-t_0)}}\breve{x}(0) \tag{20}$$

$$y(t) = C\sum_{k=0}^{n-1} \alpha_k(t)A^k\breve{x}(0) = [\alpha_0(t)\alpha_1(t)\dots\alpha_{n-1}(t)] \begin{bmatrix} C \\ CA \\ \vdots \\ CA^{n-1} \end{bmatrix} \tag{21}$$

$$\mathrm{rankQ_o} = \mathrm{rank}\begin{bmatrix} C \\ CA \\ \vdots \\ CA^{n-1} \end{bmatrix} = \mathrm{n} \tag{22}$$

The observability of the system is uniquely determined by the two coefficient matrices A and C of the state-space model, reflecting the inherent properties of the system, independent of the system inputs, disturbances, and initial state. The criterion for the observability of a multi-input system is shown in Eq. (22), where m is the rank of the C matrix.

According to the above principle of controllability and observability analysis of the state-space model, results of controllability and observability analysis for single-zone and multi-zone radiant floor models are shown in Fig. 7. It can be seen that there are many unobservable and uncontrollable states in the model and their exclusion can simplify the model structure, then the obtained reduced-order model can simplify the design and computational effort of the model predictive control.

$$\Gamma(t) = \int_0^{\infty} Ce^{A(t+\tau)}B\vartheta(t)d\tau \tag{23}$$

$$\mathrm{W}_c = \int_0^{\infty} e^{A\tau}BB^Te^{A^T\tau}d\tau \tag{24}$$

$$\mathrm{W}_O = \int_0^{\infty} e^{A^T\tau}C^TCe^{A\tau}d\tau \tag{25}$$

The first step of the balanced truncation method is to perform a model transformation to obtain the controllable Gramians matrix as shown in Eq. (24) and the observable Gramians matrix as shown in Eq. (25) of the model so that the uncontrollable states in the state-space model are transformed into unobservable states at the same time. Then the Hankel singular value (HSVs) as shown in Eq. (23) is solved by the formula $\mathrm{W}_O = \mathrm{W}_c = \sum$, which is the basis for the contribution degree of the model states to the system output. The second step is to construct the Galerkin projection of

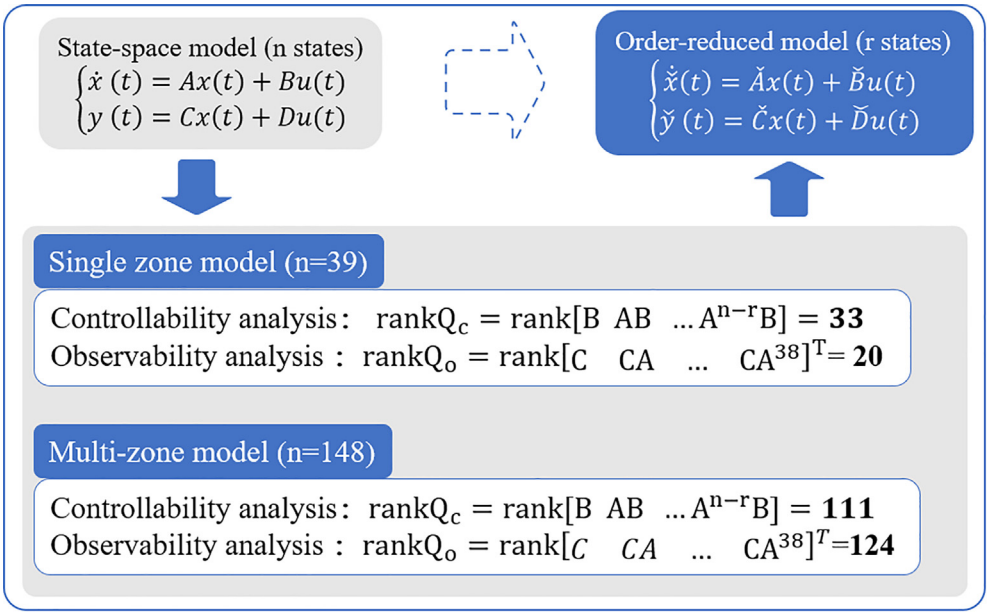

Fig. 7. Results of controllability and observability analysis for single-zone and multi-zone radiant floor models.

the model based on the Hankel singular values, and the reduced-order model obtained by applying this method can maintain the dynamic characteristics of the original model.

The 148th-order (including 148 states or temperature nodes) state-space model of the radiated floor region is downscaled using the balanced truncation method. The frequency-domain response Bode plots and Hankel singular value schematics of the full-order model, 100th-order, 26th-order, and 10th-order models are given as shown in Fig. 8(a), which contain 100, 26, and 10 states, respectively. As shown in the figure, the frequency domain response performance of the 100th-order model is almost exactly overlapped with that of the original order model, but the dimensionality of the model is not significantly reduced. When the frequency is in the range of 10^{-7}rad/s to10^{-3}rad/s, the frequency domain response performance of the full-order model and the 26th-order model match very well, with almost no difference. As the frequency increases from 10^{-3}rad/s to 10^{-2}rad/s, there is some difference in the frequency domain response of some outputs of the full-order model and the 26th-order model. When the frequency is in the range of 10^{-4}rad/s to 10^{-2}rad/s, it can be seen that the frequency domain response of the 10th-order model differs significantly from that of the original order model, as evidenced by the large difference between the blue solid line and the red solid line in the figure.

From the Hankel singular value plot of the reduced-order model, as shown in Fig. 8(b), it can be seen that the HSVs of the model gradually increase from 0 to about 1.75 as the model order decreases. The HSVs of the model with order greater than 26 is almost equal to 0, while the HSVs of the model with order less than 26 are gradually greater than 0, which indicates that the model with an order higher than 26 can keep the dynamic performance of the original model better, then the 26th-order model is selected as the final reduced-order model.

1.3. Experimental setup

The plan schematic of the experimental platform of radiant floor heating system with four thermal zones is shown in Fig. 4, the sizes of which are 4.2 m*3.6 m*2.5 m, 3.3 m*3.6 m*2.5 m, 3.0 m*3.0 m*2.5 m, 7.2 m*3.9 m* 2.5 m. The total area of the four zones is 60.18 m^2, of which 48.6 m^2 are laid with a capillary radiant floor. The total thermal resistance of the external wall, the internal wall, the radiant floor, and the ceiling are 0.86 $m^2 \cdot K/W$, 0.56 $m^2 \cdot K/W$, 0.93 $m^2 \cdot K/W$, and 0.95 $m^2 \cdot K/W$ respectively. The radiant floor is laid with integrated capillary modules for easy installation, and the system is supplied with hot water by an energy-efficient air-source heat pump, which flows through the radiant floor of the four thermal zones via a splitter and then back to the heat pump via a water mixer. The indoor air temperature in the four thermal zones is controlled individually, and the schematic diagram of the water system of the multi-zone radiant floor heating system is shown in Fig. 9.

To verify the accuracy of the reduced-order model of the radiant floor system, the parameters of radiant floor surface temperature, supply and return water temperature, indoor air temperature, and unheated internal surface temperature were tested by field experiments, and these temperatures were obtained by T-type thermocouple measurement with a measurement error of 4.44%. The supply and return water temperatures of the radiant floor were obtained by the high-precision ultrasonic calorimeter measurements, which had a measurement error of 0.10%. Besides, the outdoor ambient temperature and solar radiation intensity, etc., were monitored by an outdoor weather station as the boundary conditions of the reduced-order model during simulation. The capillary-mat radiant floor, layout diagram of temperature measurement points, and test apparatus in the experiment are shown in Fig. 10.

2. Results and discussion

The MATLAB Simulink software was used to perform the reduced-order model simulation of the multi-zone radiant floor system, and the simulation data of radiant floor surface temperature, return water temperature, indoor air temperature, and the average temperature of the unheated interior surface were obtained and compared with the test results to verify the correctness of the reduced-order model. The following figure shows the results of the experimental test, TRNSYS model, full-order model, and reduced-order model, where the grey solid line exhibits the experimental test results, the yellow one depicts the TRNSYS

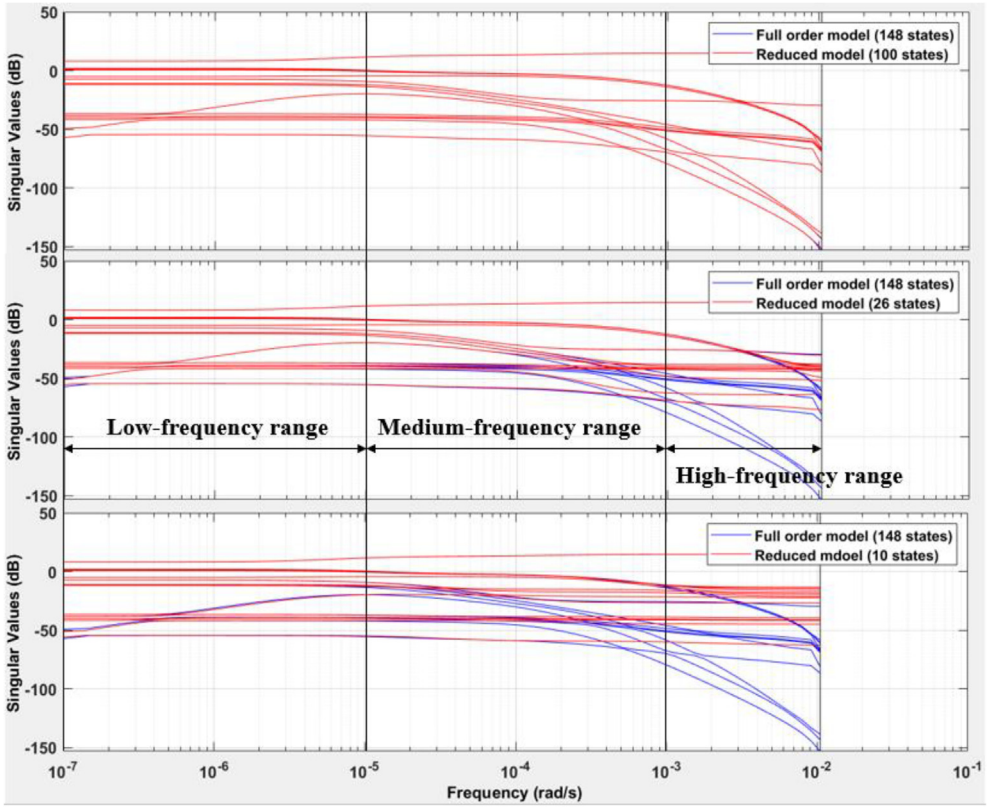

Fig. 8. (a) Frequency domain response Bode plots for different reduced-order models and (b) Hankel singular values of the reduced-order model.

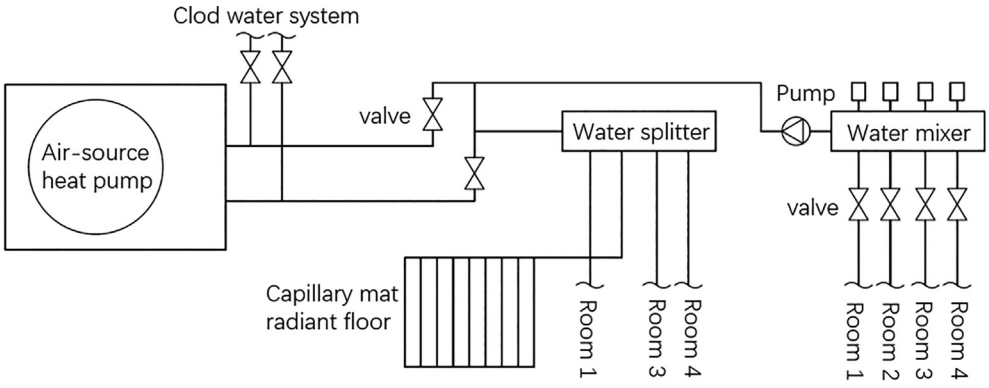

Fig. 9. Schematic diagram of the water system of the multi-zone radiant floor heating system.

(a)

(b)

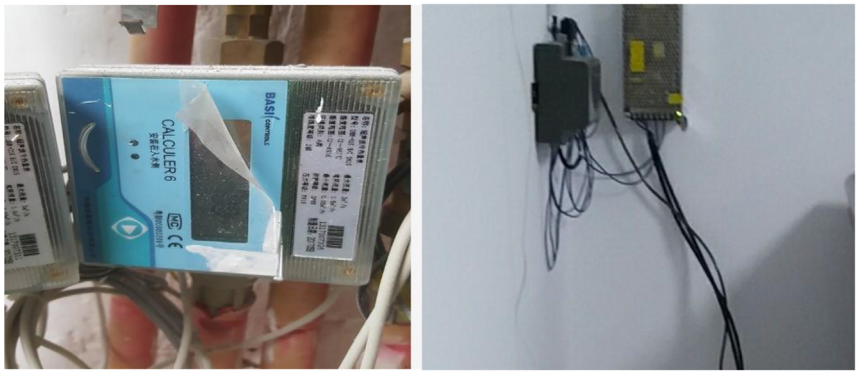

(c)

Fig. 10. (a) Capillary-mat radiant floor (b) the layout diagram of temperature measurement points, and (c) test apparatus in the experiment.

model, the blue one represents the full-order model, and the orange one represents the 26th-order model, respectively.

2.1. Accuracy analysis of the reduced-order model

Radiant floor surface temperature of four thermal zones for experimental tests, TRNSYS model, full-order model, and 26th-order model is shown in Fig. 11. It can be seen that the radiant floor surface temperature of the 26th-order model agrees well with the experimental results and is almost identical to that of the full-order model. Besides, the results of the full-order model and the 26th-order model also agree well with the results of the TRNSYS model, indicating that there is almost no difference between the modeling approach based on the state-space method and the traditional modeling based on the response factor method in terms of model accuracy, both of which are excellent.

Return water temperature of four thermal zones for experimental tests, TRNSYS model, full-order model, and 26th-order model is shown in Fig. 12. Except for the lower water temperature stage, the relative errors between the return water temperature of the three models and the experimental results gradually increase, which is still within the acceptable range. The reasons for this phenomenon are as follows: the return water temperature in the simulation results of the three models refers to the water temperature in the capillary tube in the radiant floor, while the return water temperature of the experimental test refers to the water temperature on the main pipe located after the water mixer. Therefore, the heat loss on the main pipe and the measurement error is primarily responsible for the slightly larger error in the lower water temperature stage. The reasonable and low relative errors of the radiant floor surface temperature and the return water temperature effectively demonstrate the accuracy of the reduced-order model of the radiant floor.

Zone air temperature of four thermal zones for experimental tests, TRNSYS model, full-order model, and 26th-order model is shown in Fig. 13. It can be seen that the zone temperature for

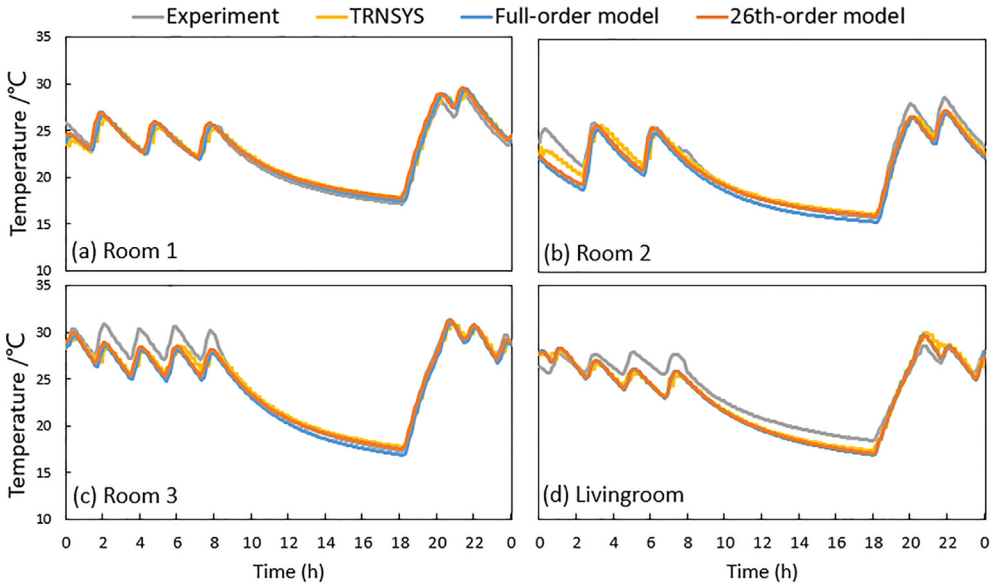

Fig. 11. Radiant floor surface temperature of four thermal zones for experimental tests, TRNSYS model, full-order model, and 26th-order model.

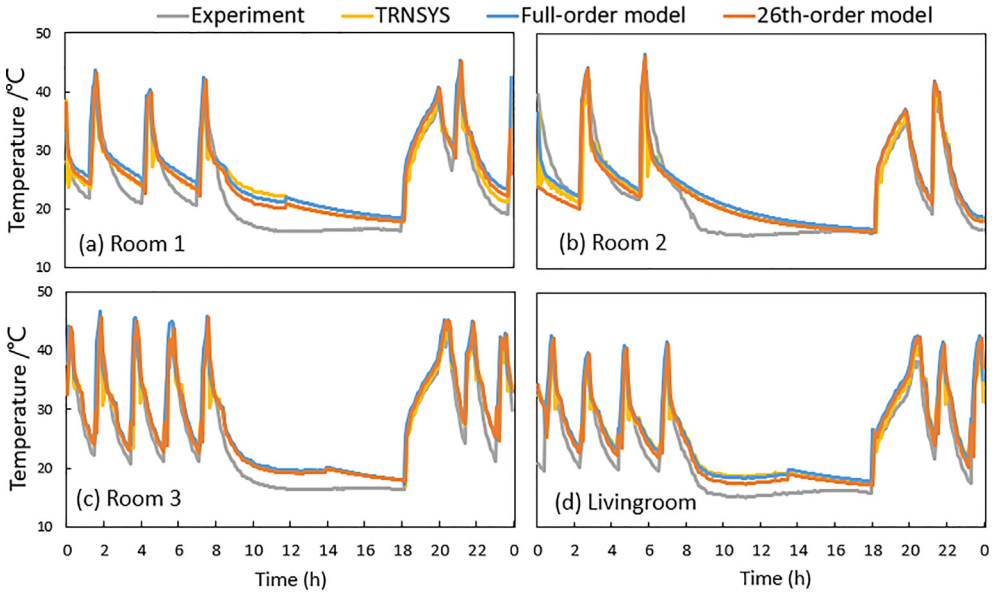

Fig. 12. Return water temperature of four thermal zones for experimental tests, TRNSYS model, full-order model, and 26th-order model.

experimental tests, TRNSYS model, full-order model, and 26th-order model agrees well with others, only that of the TRNSYS model is slightly higher than the other three. The accurate dynamic performance of the indoor air temperature model showed the great effectiveness of the reduced-order model. The radiant floor surface temperature is mainly influenced by the water supply temperature, while the indoor air temperature is the result of the coupling effect of the radiant floor model, the envelope model, and the indoor air model, which provides support to demonstrate the accuracy of the whole radiant floor thermal zone model with the precise zone air temperature.

The average unheated inner surface temperature of four thermal zones for experimental tests, TRNSYS model, full-order model, and 26th-order model is shown in Fig. 14. The average unheated inner surface temperature is the average of the five internal surface temperatures except for the radiant floor. It can be seen that the average unheated inner surface temperature for experimental tests, TRNSYS model, full-order model, and 26th-order model followed the same trend. The great agreement between the simulated and experimental test values of the internal surface temperature of the unheated envelope from the figure indicates that the linearization of the radiant heat transfer process in the model does not jeopardize the model precision.

The mean error (ERR) and root mean square error (RMSE) of the radiant floor surface temperature (T_{floor}), return water temperature (T_{wr}), zone air temperature (T_{zone}), and average internal surface temperature (T_{si}) for the four thermal zones is shown in Table 1. As can be seen, the mean error and root mean square of the radiant floor surface temperature for the 26th-order model are 0.08 °C and 0.41 °C, respectively. The mean error and root mean square of the return water temperature of the radiant floor are 3.19 °C and 4.19 °C, respectively. The mean error and root mean square of the indoor air temperature was 1.27 °C and 1.88 °C, respectively, and the mean error and root mean square of the unheated interior

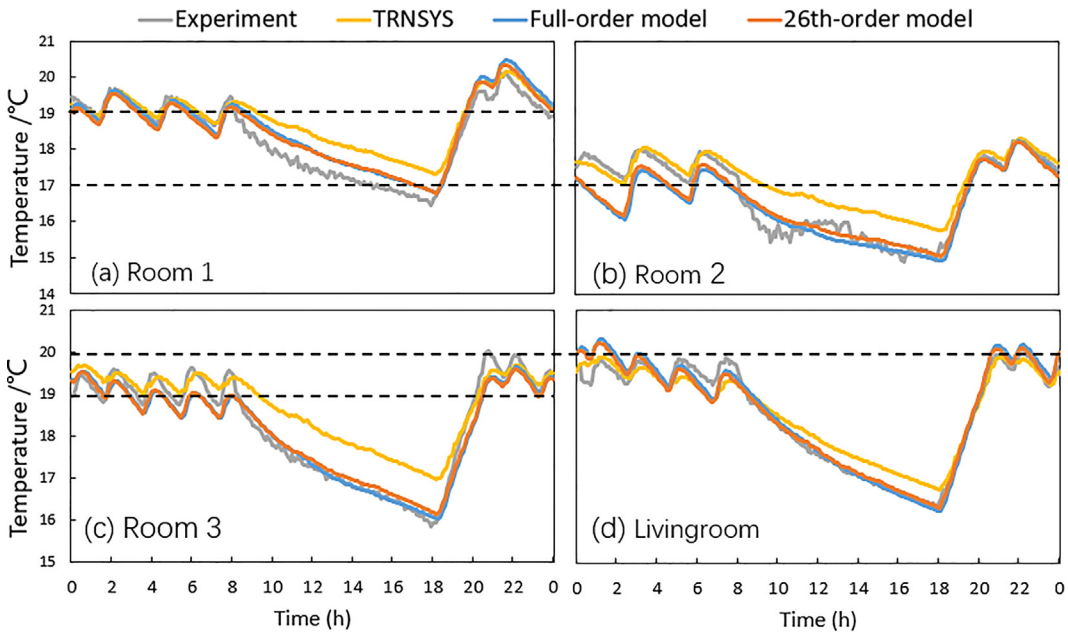

Fig. 13. Zone air temperature of four thermal zones for experimental tests, TRNSYS model, full-order model, and 26th-order model.

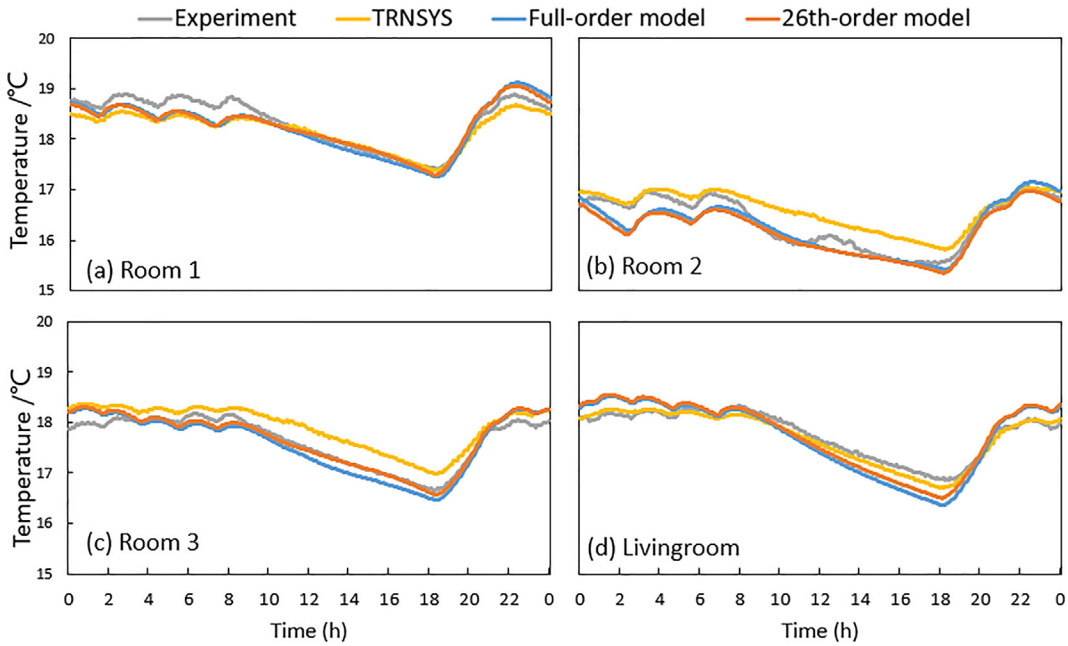

Fig. 14. Average unheated inner surface temperature of four thermal zones for experimental tests, TRNSYS model, full-order model, and 26th-order model.

surface temperature were 0.02 °C and 0.30 °C, respectively. The 26th order model has a similar level of accuracy compared to the commonly used energy simulation software TRNSYS, indicating that the 26th order model is sufficient for the simulation of radiant floor systems.

Through the above analysis of simulated values and experimental test results of the radiant floor surface temperature, return water temperature, zone air temperature, and non-heated inner surface temperature, it can be concluded that the state-space model and 26th order model of radiant floor thermal zones established in this research have great dynamic performance and reliability.

2.2. Computational efficiency analysis

Table 2 and Fig. 15(a) show the computation time comparison of the open-loop simulation for the 26th-order model, full-order model, and TRNSYS model for the radiant floor heating system when the simulation step sizes are 5 min, 10 min, and 30 min, and the simulation durations are 30 days and 365 days, respectively. The computation time for the 26th-order model ranges from 0.771 to 2 s. The computation time for the reduced-order model is so short that the effect of the simulation step size and simulation duration on the computation time is negligible. The simulation computation time for the full-order model is at most 2.5 times

Table 1
The mean error (ERR) and root mean square error (RMSE) of the radiant floor surface temperature (T_{floor}), return water temperature (T_{wr}), zone air temperature (T_{zone}), and average internal surface temperature (T_{si}) for the four thermal zones.

Tfloor	ERR(∘C)			RMSE(∘C)		
	TRNSYS model	Full-order model	26th-order model	TRNSYS model	Full-order model	26th-order model
Room1	0.42	0.22	0.16	0.58	0.35	0.44
Room2	0.41	−0.27	−0.37	0.59	0.46	0.49
Room3	0.45	−0.12	−0.16	0.65	0.29	0.38
Livingroom	0.10	0.07	0.05	0.30	0.24	0.33
Average	0.35	−0.03	−0.08	0.53	0.33	0.41
Twr	**ERR(∘C)**			**RMSE(∘C)**		
	TRNSYS model	Full-order model	26th-order model	TRNSYS model	Full-order model	26th-order model
Room1	1.86	3.01	3.89	3.53	3.58	4.69
Room2	0.60	1.53	2.50	3.18	3.01	4.58
Room3	1.51	2.22	2.72	3.26	2.63	3.03
Livingroom	2.19	2.85	3.68	3.53	3.43	4.47
Average	1.54	2.40	3.19	3.38	3.16	4.19
Tzone	**ERR(∘C)**			**RMSE(∘C)**		
	TRNSYS model	Full-order model	26th-order model	TRNSYS model	Full-order model	26th-order model
Room1	−0.56	−0.33	−0.54	1.37	1.13	1.60
Room2	−0.93	−1.71	−2.23	1.58	2.22	2.79
Room3	−0.67	−0.99	−1.45	1.27	1.28	1.79
Livingroom	−0.67	−0.82	−0.85	1.23	1.26	1.35
Average	−0.71	−0.96	−1.27	1.36	1.47	1.88
Tsi	ERR(∘C)			RMSE(∘C)		
	TRNSYS model	Full-order model	26th-order model	TRNSYS model	Full-order model	26th-order model
Room1	−0.16	−0.10	−0.08	0.22	0.19	0.25
Room2	0.23	−0.11	−0.04	0.30	0.20	0.29
Room3	0.28	−0.06	0.02	0.30	0.18	0.28
Livingroom	−0.06	−0.06	0.01	0.10	0.28	0.36
Average	0.07	−0.08	−0.02	0.23	0.21	0.30

Notes. ERR $= \sum_{k=0}^{N}(T_{simulation} - T_{experiment})/N$, RMSE $= \sqrt{\sum_{k=0}^{N}(T_{simulation} - T_{experiment})^2}/N$

Table 2
Computational time comparison of the open-loop simulation for the 26th-order model, full-order model, and TRNSYS model for the radiant floor heating system.

Step size	5 min		10 min		30 min	
Simulation durations	30 days	365 days	30 days	365 days	30 days	365 days
26th-order model (s)	1	2	0.839	1	0.771	0.909
Full-order model (s)	1	5	1	3	0.783	1
TRNSYS model (s)	11.72	109.41	6.68	55.78	5.34	20.42
26th-order model vs full-order model	0%	−60%	−16%	−67%	−2%	−9%
26th-order model vs TRNSYS model	−91%	−98%	−87%	−98%	−86%	−96%

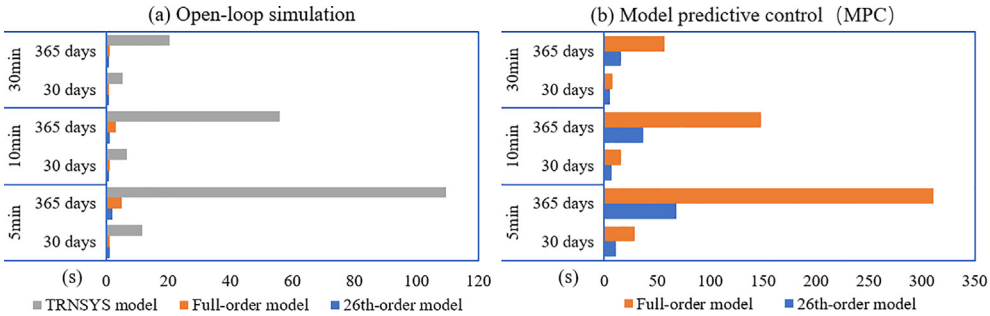

Fig. 15. Computational time comparison of the open-loop simulation and model predictive control for the 26th-order model, full-order model, and TRNSYS model for the radiant floor system.

longer than that of the 26th-order model. The computation time of the TRNSYS model ranges from 5.34 to 109.41 s. The computation time of the TRNSYS model increases significantly as the simulation step size decreases and the simulation duration increases. It can be seen that the computation time of the 26th-order model is much lower than that of the TRNSYS model for the simulation of the radiant floor, 86% to 98% lower than that of the TRNSYS model, and up to 2.5 times lower than that of the full-order model. The reduced-order model can effectively reduce the computational cost of the radiant floor model.

Model predictive control, as advanced intelligent control technology, is increasingly used in building air conditioning control systems because of its rolling optimization and good self-adaptability. Model predictive control has tight requirements on the computation effort of predictive models, and the redundant computation of complex predictive models is bound to a degradation in the robustness of model predictive control. Table 3 and

Table 3
Computational time comparison of model predictive control (MPC) for the 26th-order model and full-order model for the radiant floor heating system.

Step size	5 min		10 min		30 min	
Simulation durations	30 days	365 days	30 days	365 days	30 days	365 days
26th-order model (s)	11	68	7	37	5	16
Full-order model (s)	29	311	16	148	8	57
Relative ratio	−62%	−78%	−56%	−75%	−38%	−72%

Fig. 15(b) show the computational time comparison of model predictive control (MPC) for the 26th-order model and full-order model for the radiant floor heating system when the simulation step sizes are 5 min, 10 min, and 30 min, and the simulation durations are 30 days and 365 days, respectively. By comparing with Table 2, it was found that the simulation time of the radiant floor system with model predictive control increased significantly. The simulation time for the full-order model ranged from 8 to 311 s, while the simulation time for the 26 models was only between 5 and 68 s. The 26th-order model used for model predictive control can effectively reduce the simulation time by 38%~78% compared to the full-order model, reducing the simulation time and CPU load on the computer, greatly improving the computational efficiency of model predictive control, and therefore strengthening the response performance and enhancing the robustness of model predictive control. The focus of this research is to improve the computational efficiency of the radiant floor system by developing the reduced-order model, and more in-depth studies on the dynamic properties of the model predictive control system are expected to be further developed in the future.

3. Conclusion

To address the problem that advanced model predictive control requires high computational efforts, a fast and high-fidelity reduced-order model of a multi-zone radiant floor system is proposed by applying the efficient balanced truncation method which is commonly used in modern control research field. Based on Hankel singular derived from the controllability and observability analysis and the frequency-domain response bode plots of the model, a reduced-order model is obtained that accurately characterizes the dynamic performance of the system with much lower computational effort. The accuracy of the reduced-order model is verified by comparing it with the experimental test results, the TRNSYS model, and the original order model. Besides, the reduced-order model can greatly improve the robustness of the model predictive control system.

The following conclusions can be drawn: (2) The 26th-order model of the multi-zone radiant floor system was obtained based on the HSVs of the balanced truncation method from the full-order model, which is sufficient to characterize the dynamic thermal performance of the original model. (3) The radiant floor surface temperatures, return water temperature, zone air temperature, and the average internal surface temperature of the unheated envelopes of the 26th-order model are in high agreement with the experimental results, TRNSYS model, and the full-order model, proving the high precision and accuracy of the 26th-order model, where the root mean square errors are 0.41℃, 4.19℃, 1.88℃, and 0.30℃, respectively. (3) The computational time for the open-loop simulation of the 26th-order model was reduced by 86% to 98% compared to that of the TRNSYS model. The computational time for the model predictive control of the 26th-order model was significantly reduced by 38%~78% compared to that of the full-order model, which greatly reduces the simulation time and CPU load on the computer, improving the computational efficiency of model predictive control, and therefore strengthening the response performance and enhancing the robustness of model predictive control.

Declaration of Competing Interest

The authors declare that they have no known competing financial interests or personal relationships that could have appeared to influence the work reported in this paper.

References

[1] Q. Chen, N. Li, W. Feng, Model predictive control optimization for rapid response and energy efficiency based on the state-space model of a radiant floor heating system, Energy Build. 238 (2021) 110832.
[2] M.M. Gouda, S. Danaher, C.P. Underwood, Building thermal model reduction using nonlinear constrained optimization, Build. Environ. 37 (12) (2002) 1255–1265.
[3] Tianzhen H, Y.J., A new multi-zone model for the simulation of building thermal performance. Building and Environment, 1997. 32(2), p123-128.
[4] C. Ménézo, J.J. Roux, J. Virgone, Modelling heat transfers in building by coupling reduced-order models, Build. Environ. 37 (2) (2002) 133–144.
[5] C.R. Touretzky, M. Baldea, Nonlinear model reduction and model predictive control of residential buildings with energy recovery, J. Process Control 24 (6) (2014) 723–739.
[6] J. Wang et al., Predicting home thermal dynamics using a reduced-order model and automated real-time parameter estimation, Energy Build. 198 (2019) 305–317.
[7] W. Devia, K. Agbossou, A. Cardenas, An evolutionary approach to modeling and control of space heating and thermal storage systems, Energy Build. 234 (2021) 110674.
[8] V.S.K.V. Harish, A. Kumar, Reduced order modeling and parameter identification of a building energy system model through an optimization routine, Appl. Energy 162 (2016) 1010–1023.
[9] J. Berger et al., Proper Generalised Decomposition for heat and moisture multizone modelling, Energy Build. 105 (2015) 334–351.
[10] J. Berger et al., Review of Reduced Order Models for Heat and Moisture Transfer in Building Physics with Emphasis in PGD Approaches, Arch. Comput. Methods Eng. (2016) 1–13.
[11] M. Heidarinejad et al., Demonstration of reduced-order urban scale building energy models, Energy Build. 156 (2017) 17–28.
[12] S. Heo, Nonlinear control of high duty counter-current heat exchangers using reduced order model, Appl. Therm. Eng. 157 (2019) 113720.
[13] Z. Shi, W. O'Brien, Building energy model reduction using model-cluster-reduce pipeline, J. Build. Perform. Simul. 11 (5) (2018) 553–567.
[14] M.H. Shamsi et al., A generalization approach for reduced order modelling of commercial buildings, Energy Procedia 122 (2017) 901–906.
[15] M. Georgescu, I. Mezic, Building energy modeling: A systematic approach to zoning and model reduction using Koopman Mode Analysis, Energy Build. 86 (2015) 794–802.
[16] X. He, Q. Kong, Z. Xiao, Fast simulation methods for dynamic heat transfer through building envelope based on model-order-reduction, Procedia Eng. 121 (2015) 1764–1771.
[17] Q. Kong, X. He, Y. Jiang, Fast simulation of dynamic heat transfer through building envelope via model order reduction, Build. Simul. 10 (003) (2017) 419–429.
[18] T. Hou, S. Roels, H. Janssen, Model order reduction for efficient deterministic and probabilistic assessment of building envelope thermal performance, Energy Build. 226 (2020) 110–366.
[19] A. Tallet, L. Erwan, C. Inard, Fast POD method to evaluate infiltration heat recovery in building walls, Build. Simul. 10 (2016) 10–36.
[20] J. Zhang et al., Three-dimensional magnetotelluric modeling using the finite element model reduction algorithm, Comput. Geosci. 151 (2021) 104750.
[21] S. Goyal, P. Barooah, A method for model-reduction of non-linear thermal dynamics of multi-zone buildings, Energy Build. 47 (2012) 332–340.
[22] E.-J. Kim et al., Fast and accurate district heating and cooling energy demand and load calculations using reduced-order modelling, Appl. Energy 238 (2019) 963–971.
[23] B. Lyons, E. O'Dwyer, N. Shah, Model reduction for Model Predictive Control of district and communal heating systems within cooperative energy systems, Energy 197 (2020) 117–178.

[24] Černý, R.H., Tianfeng Roels, Staf, Janssen, Hans, Kočí, J., Kočí, V. The use of proper orthogonal decomposition for the simulation of highly nonlinear hygrothermal performance. in MATEC Web of Conferences. 2019.
[25] T. Hou et al., The use of POD–DEIM model order reduction for the simulation of nonlinear hygrothermal problems, E3S Web of Conferences 172 (2020) 04002.
[26] T. Hou et al., POD–DEIM model order reduction for nonlinear heat and moisture transfer in building materials, J. Build. Perform. Simul. 13 (6) (2020) 645–661.
[27] Hou, T., S. Roels,H. Janssen. A comparison of model order reduction methods for the simulation of wall heat transfer. in Healthy, Intelligent and Resilient Buildings and Urban Environments. 2018.
[28] E. Palomo Del Barrio et al., Using model size reduction techniques for thermal control applications in buildings, Energy Build. 33 (1) (2000) 1–14.
[29] D. Pernsteiner et al., Data-based model reduction for phase change problems with convective heat transfer, Appl. Therm. Eng. (2020) 116228.
[30] P. Wang et al., Reduction analysis of building thermal models for simulation of heating accidents, Build. Simul. 13 (6) (2020) 1249–1258.
[31] W.J. Cole et al., Reduced-order residential home modeling for model predictive control, Energy Build. 74 (2014) 69–77.
[32] D. Kim, J.E. Braun, A general approach for generating reduced-order models for large multi-zone buildings, J. Build. Perform. Simul. 8 (6) (2014) 435–448.
[33] Y. Wang et al., Accurate model reduction and control of radiator for performance enhancement of room heating system, Energy Build. 138 (2017) 415–431.
[34] Yi, J., State-space method for the calculation of airconditioning loads and the simulation of thermal behaviour of the room. ASHRAE Transactions, 1981. 88 (2): p. : 122~132.
[35] D. Kim, J.E. Braun, Reduced-order building modeling for application to model-based predictive controL, Proceed. SimBuild (2012) 8.
[36] N. Nord et al., Data informed physical models for district heating grids with distributed heat sources to understand thermal and hydraulic aspects, Energy 222 (2021) 119965.
[37] J. Hartnett, Rohsenow, Warren, Handbook of Heat Transfer, 1973.
[38] V. Paschkis, H.D. Baker, A method for determining unsteady state heat transfer by means of an electrical analogy, Trans. ASME 64 (1942) 105–112.
[39] B.C. Moore, Principal component analysis in linear systems: Controllability, observability, and model reduction, IEEE Trans. Autom. Control 26 (1) (1981) 17–32.
[40] Q. Li et al., Effective and scalable modelling of existing non-domestic buildings with radiator system under uncertainty, J. Build. Perform. Simul. 13 (6) (2020) 740–759.
[41] R. Stanisławski, M. Rydel, K.J. Latawiec, Modeling of discrete-time fractional-order state space systems using the balanced truncation method, J. Franklin Inst. 354 (7) (2017) 3008–3020.
[42] Y. Yao et al., Modular modeling of air-conditioning system with state-space method and graph theory, Int. J. Refrig 99 (2019) 9–23.
[43] J. Deng et al., Effectiveness of the thermal mass of external walls on residential buildings for part-time part-space heating and cooling using the state-space method, Energy Build. 190 (2019) 155–171.
[44] J. Shair et al., Modeling and stability analysis methods for investigating subsynchronous control interaction in large-scale wind power systems, Renew. Sustain. Energy Rev. 135 (2021) 110420.